Supporting Information Apparent phototaxis enabled by BM

Lukas Niese[a], Linlin Wang[a], Sayan Das[b], and Juliane Simmchen*[a]

[a]Physical Chemistry, TU Dresden, Zellescher Weg 19, 01069 Dresden, Email: juliane.simmchen@tu-dresden.de
[b]MPI Intelligent Systems, Heisenbergstr. 3 70569 Stuttgart

1 Videos

List of Videos:
Video S1 0.7 µm Au@Ni@TiO_2 in 0.5 % H_2O_2 at lamp power of 315 mW UV light
Video S2 1.2 µm Au@Ni@TiO_2 in 0.5 % H_2O_2 at lamp power of 315 mW UV light
Video S3 1.6 µm Au@Ni@TiO_2 in 0.5 % H_2O_2 at lamp power of 315 mW UV light
Video S4 3.5 µm Au@Ni@TiO_2 in 0.5 % H_2O_2 at lamp power of 315 mW UV light

2 Additional experimental details

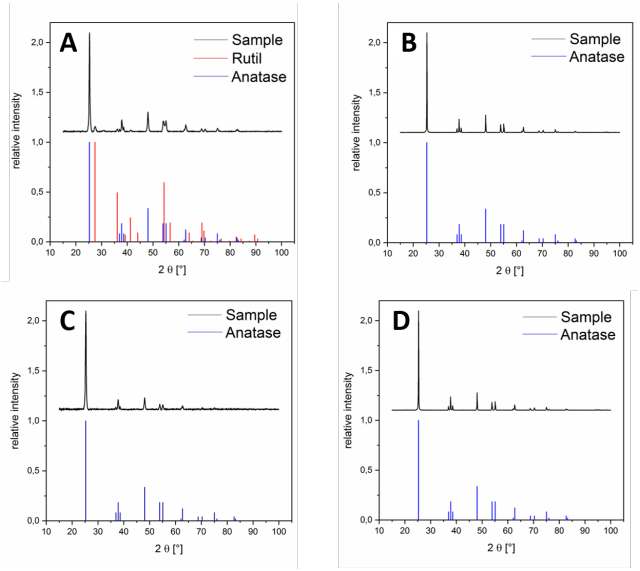

Figure S1: Results of powder XRD measurements of the 4 particle samples with average sizes of **A** 0.7 µm, **B** 1.2 µm, **C** 1.6 µm and **D** 3.5 µm. The coloured lines show, the typical XRD patterns of pure anatase and rutile phases taken from database

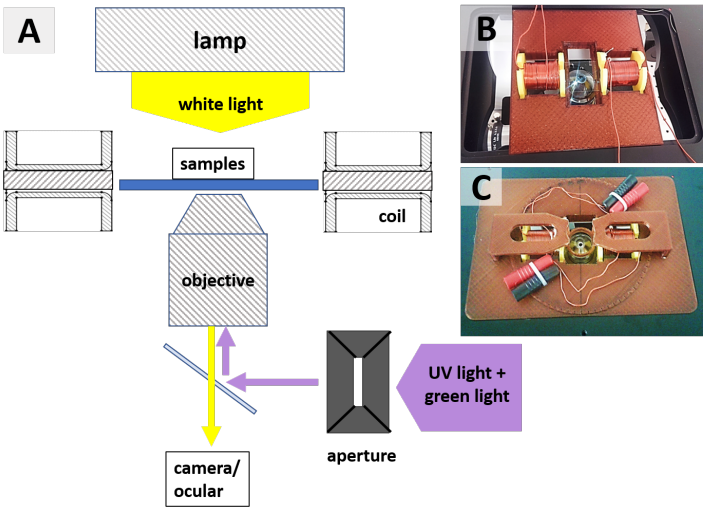

Figure S2: **A**, schematical illustration of microscope apparatus with light paths of white light (yellow) and green + UV light in purple. **B** and **C**, pictures of self designed mountings for magnetic coils and cover glass on the microscope platform. **C** is equipped with a turnable disc for free adjustment of the magnetic field direction in plane. Both pictures show the typical alignment for vertical particle movement according to the figures in main text.

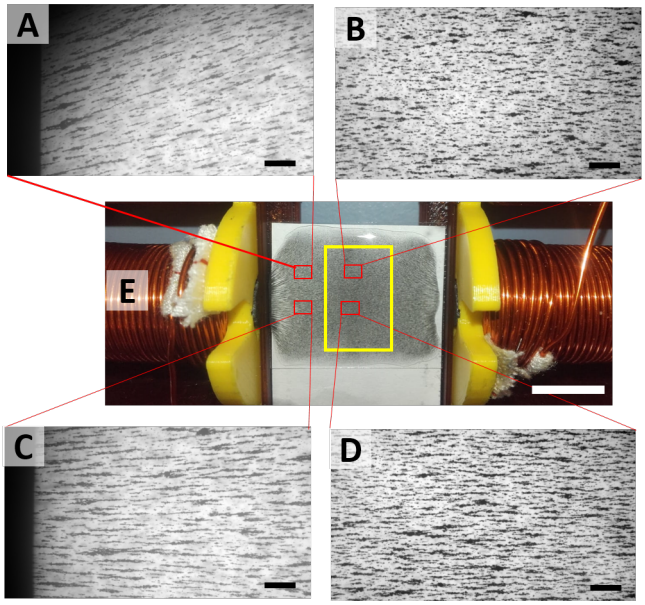

Figure S3: Fieldlines of magnetic coil setup with $\overrightarrow{B} = 5$ mT at different positions of cover glass. **E** yellow rectangle marks area with mostly homogeneous field, which was used for experimental operations

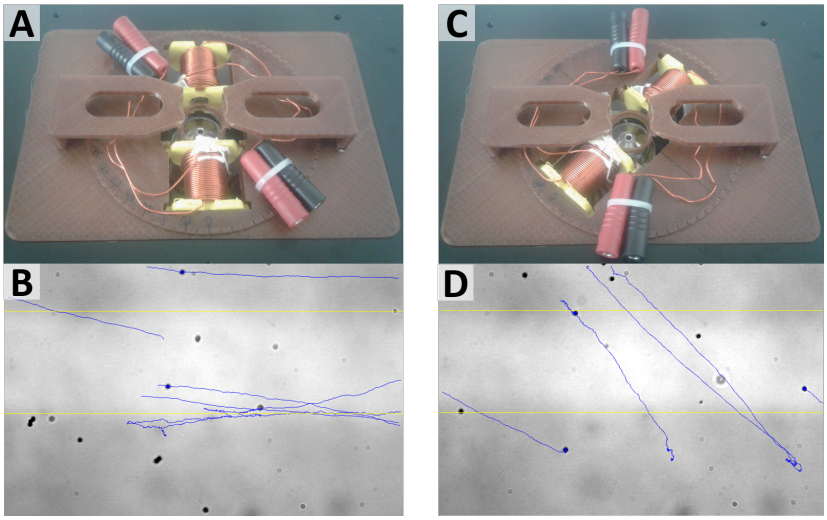

Figure S4: Particle tracks with different orientations of magnetic field. **B**, fieldlines in 90° angle towards horizontal axis. **D**, fieldlines in 45° angle towards horizontal axis. **A** and **C** show, alignment of magnetic coils for experiments **B** and **D**

.

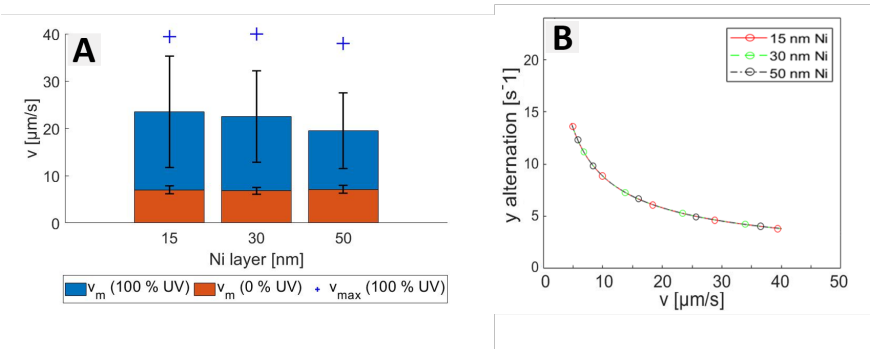

Figure S5: Independence of particle behaviour towards thickness of Ni layer. **A** shows the typical velocities of 0.7 μm sized particles with different covering thicknesses of Ni. **B**, illustrates the tendency of the three samples in **A** to switch their movement direction according to vertical axis (y).

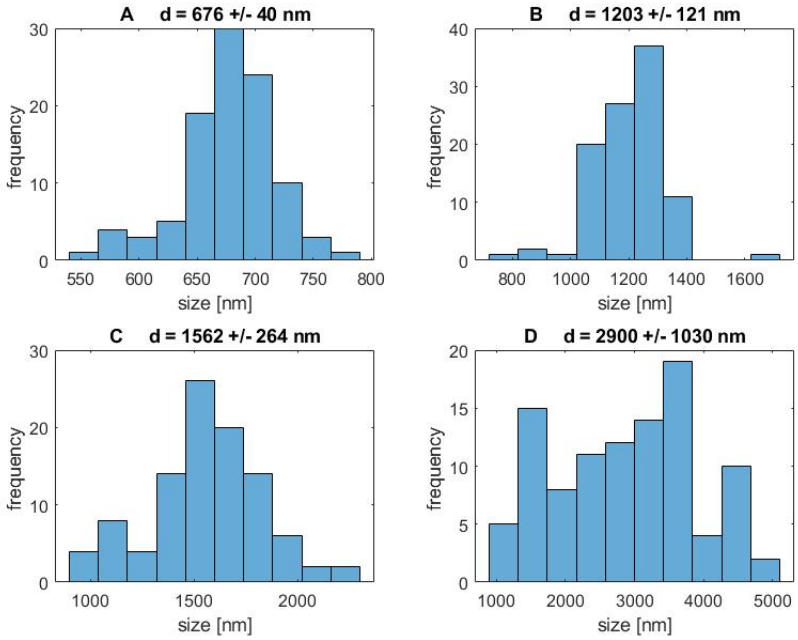

Figure S6: Histogram of size distribution for the 4 particle batches with nominal sizes of 0.7 µm (A), 1.2 µm (B), 1.6 µm (C) and 3.5 µm (D).

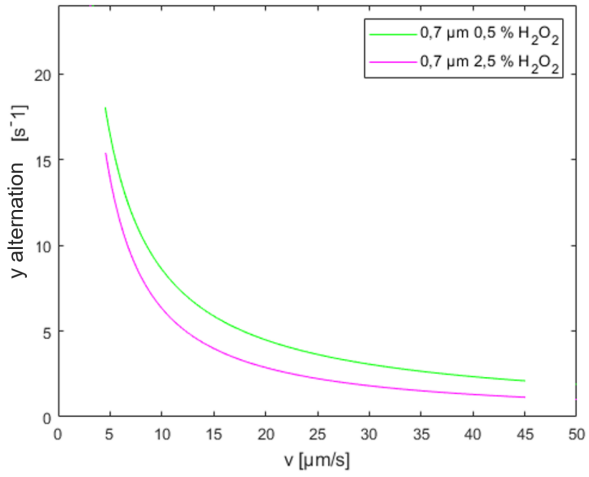

Figure S7: Tendency of turning back, depending on velocity for 0.7 µm particle under 2 different concentrations of hydrogen peroxide.

Condition	**Illustration**	**Φ [°]**	**Θ [°]**	**Motion**
No activity, no constraints through any external influences	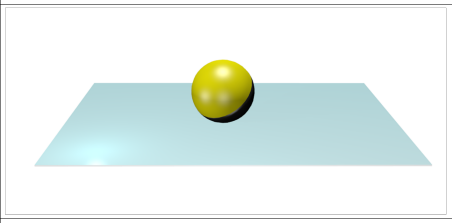	Not restricted	Not restricted	Brownian motion
No activity, magnetic field B in Y direction	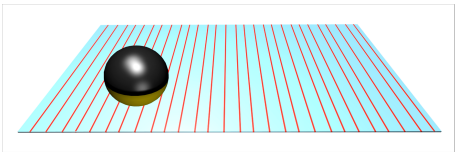	Magnetic moment of the cap is aligned with B, Φ ∥ B	Not restricted	Restricted Brownian motion
Activity without any external field		Not restricted	Θ = -$\pi/2$, $\pi/2$	Ballistic motion of random orientation
Activity in magnetic field	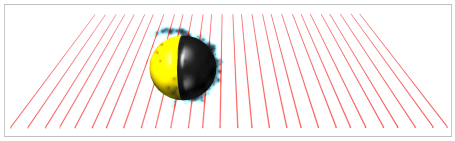	Fixed at Φ ∥ B	Θ = -$\pi/2$, $\pi/2$	Ballistic motion directed by B

Figure S8: The magnetic field as well as the activity influence the orientation of the particle, all influences and the angles are detailed here.

.

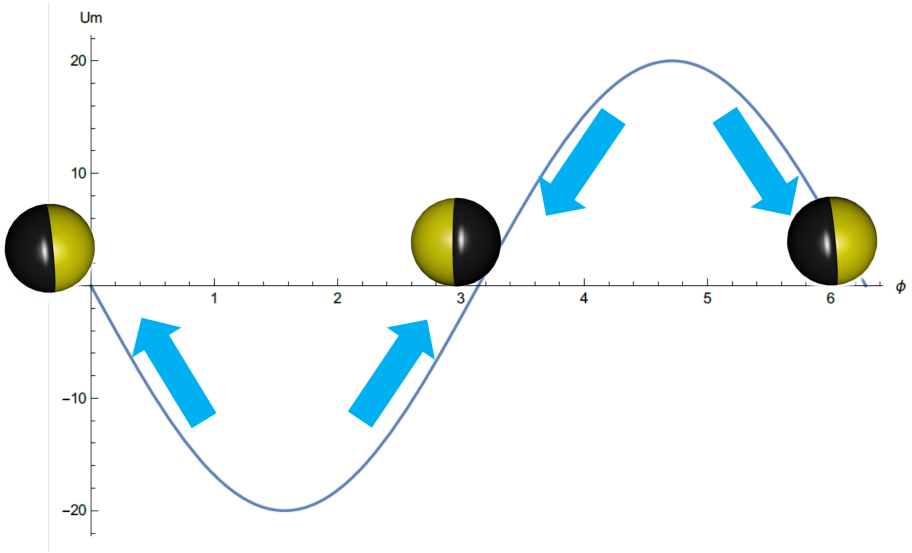

Figure S9: The magnetic field creates a sinusoidal potential that becomes 0 only if the particle's cap is aligned with B. This is the case for $\phi = n*\pi$ meaning any rotation around the y axis maintaining the cap orientation parallel to B is allowed

.

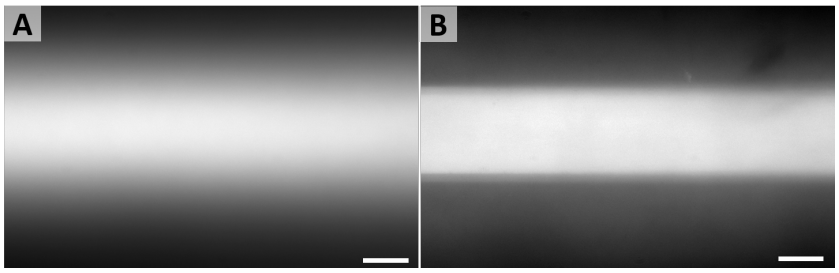

Figure S10: Light restricted by aperture. **A** visualized UV-light by fluorescent pyranin dye **B** visible green light without addition of UV fraction

To check the delimitation of UV light, an thin film of agar containing 0.1 mM Pyranin as fluorophore was spread over a glass slide (Fig. S10 **A**). The agar was used to fix the dye molecules in a matrix and prevent diffusion of exited molecules. In comparison with the same area irradiated only by green light, the UV-light is observable in a wider stripe. This matches with the detected photo-catalytic activity of particles at the edges of the stripe and could be explained by Rayleighscattering, which is stronger with light of shorter wavelength.

3 Additional information on the theoretical approach

3.1 Particle Configuration and Phase Portraits

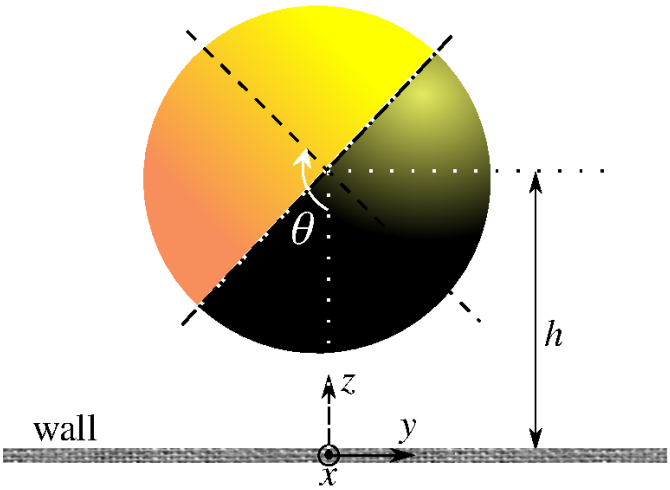

Figure ST1: The particle configuration used for calculating phase portraits depends mainly on the particle height h and the angle θ.

In order to obtain phase portraits, first we need knowledge of the particle velocity $\mathbf{U}$ and $\mathbf{\Omega}$. This particle velocity comprises of both the effects of self-propulsion and gravity induced sedimentation (see details in 3.2). The self-propulsion velocity counterpart is obtained by the utilizing the classical theory of diffusophoresis along with the help of a numerical approach that has been previously used by Uspal et al. [2]. The contribution due to gravity is obtained directly from the gravitational force and torque acting on the particle. The particle velocity is calculated corresponding to a grid of values of (h, θ) that refer to different particle configurations. Next, to obtain the particle trajectories for different initial configurations, numerical integration is done by interpolating $\dot{\bar{h}} = U_y,\ \dot{\theta} = -\Omega_x$, where $\bar{h} = hR$, R being the particle radius. The calculations are carried out for $h \geq 1.02$ to prevent any loss of any numerical accuracy. These trajectories gives us a better visualization of the particle dynamics and are represented in the form of the phase portraits.

3.2 Parameters F and T

In this manuscript, phase portraits are obtained for particles at different dynamic situations. For that, both the parameters F and T play an important role in determining the particle dynamics. The parameter F denotes the apparent weight of the particle in the peroxide solution whereas T signifies the gravitactic torque. Both of these parameters are scaled with respect to the Stokes force and the corresponding torque acting on the particle, respectively. To determine these parameters details of the geometry of the catalytic cap is required. For the present model, an"egg-shell" geometry is utilized [1] and is shown in the schematic below. The cap here comprises of a composite layer of Nickel (Ni) and Gold (Au), whose maximum thickness at the pole are δ_{Ni} and δ_{Au} respectively. With the consideration that $(\delta_{Ni} + \delta_{Au})/R \ll 1$, the mass of the (lens-shaped) composite cap can be shown to be: $m_c = 2\pi(\delta_{Ni} + \delta_{Au})R^2\rho_c/3$, where ρ_c is the density of the composite cap. The center of the mass of this cap can be shown to be located at a distance of $d_{com} = 0.75\,\{R + 0.5(\delta_{Ni} + \delta_{Au})\}$ from the center of the core sphere, O. Since the cap is very thin, the entire particle can be considered to possess a spherical shape of radius R and also any deviation of the center of mass of the particle from the centroid O of the spherical core is neglected. Under such circumstances, the torque due gravity acts on the particle solely due to the presence of the composite cap.

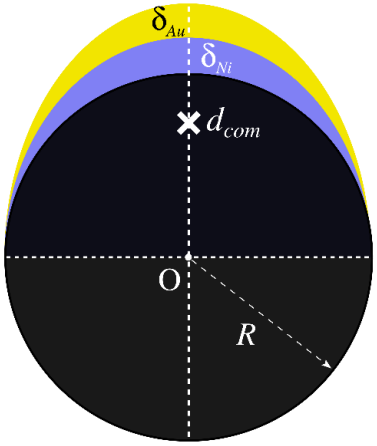

Figure ST2: Schematic of the cross-section of a model "egg-shell" active particle. The black colored disc of radius R denotes the TiO_2 core, whereas the blue and gold lens-shaped region denote the Nickel and Gold cap respectively. d_{com} is the distance of the center of mass of the composite cap from the centroid O.

References

[1] Andrew I. Campbell and Stephen J. Ebbens. Gravitaxis in spherical janus swimming devices. *Langmuir*, 29(46):14066–14073, 2013. PMID: 24134682.

[2] W. E. Uspal, M. N. Popescu, S. Dietrich, and M. Tasinkevych. Self-propulsion of a catalytically active particle near a planar wall: from reflection to sliding and hovering. *Soft Matter*, 11:434–438, 2015.